JoT JOURNAL OF TURBULENCE

http://jot.iop.org/

Vertical transport of heat and momentum across a sheared density interface at the top of a horizontally evolving convective boundary layer†

Evgeni Fedorovich[1,2] **and Johannes Thäter**[2]

[1] School of Meteorology, University of Oklahoma, Norman, OK 73019, USA
[2] Institute for Hydromechanics, University of Karlsruhe, Karlsruhe 76128, Germany
E-mail: fedorovich@ou.edu and thaeter@ifh.bau-verm.uni-karlsruhe.de

Received 27 February 2001; online 11 April 2001

Abstract. The turbulence regime in a quasi-stationary, horizontally evolving, and sheared boundary layer with bottom buoyancy forcing has been studied numerically by means of large eddy simulations (LES) in conjunction with its experimental investigation in a laboratory wind tunnel. The atmospheric prototype of the investigated boundary layer is commonly observed in the earth's atmosphere during daytime conditions. In meteorology, a boundary layer of this kind is usually called the convective boundary layer (CBL). The case studied of a horizontally evolving CBL corresponds to the boundary layer flow that develops in a stably or neutrally stratified air mass advected over a heated underlying surface.

A characteristic feature of the CBL case studied is the presence of wind shear across the capping temperature inversion (density interface) at the CBL top. This elevated wind shear affects the CBL turbulence structure in combination with the shear and buoyancy sources at the underlying surface. This study has focused on the convective entrainment and the CBL growth dynamics under the combined influence of all mentioned forcings.

It has been found that entrainment of momentum across the sheared inversion can accelerate or decelerate the mean flow in the main portion of the CBL depending on the sign of elevated shear. The induced flow convergence/divergence below the inversion leads to local organized ascending/descending motions that considerably modify the CBL growth rate. The turbulence structure throughout the whole CBL is also noticeably affected by these motions.

PACS numbers: 92.60.Fm, 47.27.Eq, 47.27.Nz, 47.27.Te

† This article was chosen from selected Proceedings of the Eighth European Turbulence Conference (*Advances in Turbulence VIII (Barcelona, 27–30 June 2000)* (Barcelona: CIMNE) ed C Dopazo. ISBN: 84-89925-65-8).

©2001 IOP Publishing Ltd PII: S1468-5248(01)22931-2 1468-5248/01/000001+17$30.00

JoT 2 (2001) 007

Contents

1. Introduction

Turbulent flow in the atmospheric convective boundary layer (CBL) is a natural example of a buoyantly driven boundary-layer flow with velocity (or wind) shear. The buoyancy forcing in the atmospheric planetary boundary layer is commonly represented by convective heat transfer from a warm underlying surface. This feature is an apparent reason for calling the considered boundary layer type 'convective' in the geophysical applications of fluid mechanics. The term 'convective' also emphasizes the fact that buoyant convection is the main mechanism of turbulence production in the CBL, whilst the contribution of wind shear to the generation of turbulence is of secondary importance.

The convective forcing generates up- and downward motions that effectively mix momentum and scalar fields inside the CBL. Due to such mixing, the wind and temperature fields in the main portion of the CBL (the so-called convectively mixed layer) do not change considerably with height when averaged over horizontal planes, or over time. In meteorology, the upward convective motions, or updrafts, are commonly referred to as convective thermals. The fast rising convective thermals occupy a lower percentage of the CBL horizontal cross-sectional area than the broader, but slower descending convective motions, or downdrafts.

The mixed core of the CBL is separated from the underlying surface and from the free atmosphere aloft by comparatively narrow sublayers. In the lower region of the CBL, the surface (sub)layer is located. Throughout this layer, the mean flow temperature and velocity change with height in a relatively sharp way. Another sublayer with comparatively sharp vertical variations of mean flow characteristics is located close to the CBL top, where the density interface separates the CBL from the outer free-atmospheric flow. The density interface in the atmospheric CBL appears as a flow region with inverse vertical temperature gradient. Due to this, it is usually called the capping inversion layer (or simply the capping inversion). Wind shear at the surface and wind shear across the inversion layer (also called surface wind shear and elevated wind shear, respectively) contribute to the CBL turbulence regime in conjunction with the dominant convective forcing.

Interaction between the CBL and the outer flow is manifested by the entrainment of heat and momentum across the capping inversion layer down into the convectively mixed core of the CBL. The entrainment is maintained by flow disturbances resulting from the penetration of convective thermals into stably stratified fluid above the CBL.

Data from the classic field studies of atmospheric CBL by Clarke *et al* [1], Kaimal *et al* [2], Caughey and Palmer [3], and Lenschow *et al* [4] are widely used to verify models and

JoT 2 (2001) 007

parametrizations of the CBL. However, the interpretation of atmospheric field data is severely complicated by the combined effect of wind shear, advection, large-scale subsidence, and gravity waves on the turbulence structure in the atmospheric CBL. These complications stipulated the scientific interest towards laboratory and numerical CBL studies that provide an opportunity to single out and separately quantify effects of different CBL flow forcings.

From the viewpoint of historical retrospective, the non-steady shear-free atmospheric CBL is the most extensively studied CBL case. The turbulence structure in a CBL of this type is assumed to be statistically homogeneous in the horizontal. It was successfully simulated in laboratory water tanks by Deardorff *et al* [5, 6], Willis and Deardorff [7], Deardorff and Willis [8], Adrian *et al* [9], Kumar and Adrian [10], and Cenedese and Querzoli [11], and studied numerically, using the large eddy simulation (LES) technique, by Deardorff [12], Moeng [13], Wyngaard and Brost [14], Nieuwstadt and Brost [15], Mason [16], and Schmidt and Schumann [17] among others.

The last decade has been marked by application of LES in the studies of variety of driving mechanisms of the non-steady CBL. In particular, the effects of wind shear on the turbulence regime in the non-steady CBL have been numerically investigated by Mason [18], Moeng and Sullivan [19], and Khanna and Brasseur [20].

It is necessary to mention, however, that besides the non-steady CBL there is another CBL case commonly observed in geophysical flows. This is the case of a horizontally evolving CBL. Such a boundary layer develops in a stratified fluid advected over a heated underlying surface. In many instances, turbulent flow in the horizontally evolving CBL may be considered quasi-stationary. Turbulence properties in this CBL case are much less understood than those of the non-steady CBL. Only recently, laboratory and numerical studies have been conducted that provided a quantitative description of the turbulence regime in the horizontally evolving CBL, see Fedorovich *et al* [21], Kaiser and Fedorovich [22], Fedorovich and Kaiser [23], Ohya *et al* [24], Ohya and Uchida [25], Fedorovich *et al* [26, 27].

The role of wind shears in the CBL turbulence regime also deserves additional investigation. In the majority of reported studies of the sheared CBL, the emphasis has been laid on the surface shear whilst the effects of elevated wind shear on the CBL evolution and turbulent transport across the capping inversion have not been sufficiently addressed. Fedorovich and Kaiser [23] presented results from a series of laboratory experiments with the sheared CBL in the stratified wind tunnel of the University of Karlsruhe (UniKa). In their experimental set-up for the CBL with sheared capping inversion, the mean flow velocity above the inversion was larger than in the convectively mixed region below the inversion. Such elevated wind shear was found to produce a double-sided effect on the dynamics of the horizontally developing CBL. From one side, it led to the pronounced turbulence enhancement in the upper portion of the CBL. From the other side, the CBL with elevated shear grew noticeably slower than the CBL with the shear-free upper interface.

Fedorovich *et al* [27] tried to associate this damping effect of elevated shear on the CBL growth with the so-called shear sheltering of turbulence previously discussed in Csanady [28], Jacobs and Durbin [29], Hunt [30], and Hunt and Durbin [31]. In the numerical part of their study, Fedorovich *et al* [27] discovered what they called the directional effect of elevated shear on the growth of the horizontally evolving CBL. In the case of positive wind shear across the inversion layer (the flow above the inversion possesses a larger momentum than mean motion in the mixed layer), the CBL growth has been found to be impeded compared to the case of CBL with the shear-free inversion. Hence, numerical support has been provided to the earlier experimental findings of Fedorovich and Kaiser [23] regarding the damping effect of positive shear on the CBL development. On the other hand, the numerical experiments of Fedorovich *et al* [27] revealed the activation of boundary layer growth in the case of elevated negative shear

JoT 2 (2001) 007

when the mean flow above the inversion possesses a smaller horizontal momentum than mean motion in the mixed layer. In this way, the effect of negative elevated shear on the CBL growth turned out to be opposite to that of the positive shear.

The authors of [27] failed to interpret the directional effect of elevated wind shear within the framework of shear sheltering theory developed by Hunt and Durbin [31]. However, Fedorovich *et al* [27] proposed a physical explanation for the discovered influence of shear on the CBL dynamics based on their own considerations of distortion of convective thermals penetrating into the stably stratified environment in the presence of elevated wind shears of different sign. It will become clear from the following analyses that this explanation can by no means be regarded sufficient.

In the present paper, we show and discuss new numerical data on the turbulence structure and integral parameters of the horizontally evolving CBL in the presence of elevated wind shears. Some new data from the wind tunnel experiments on the dispersion of passive scalar in the CBL capped by sheared interface will also be invoked. Our objectives are (i) to investigate the effect of elevated shear and associated entrainment of momentum across the sheared inversion on the interaction between the organized and turbulent components of motion in the horizontally evolving CBL and (ii) to narrow gaps in the preceding physical analyses of the modification of CBL dynamics by elevated wind shears.

The employed LES procedure and the basic features of the wind tunnel experimental technique are briefly described in section 2 of the paper. Examples of mean flow patterns and distributions of turbulence statistics in the simulated CBL with elevated wind shears of different signs will be presented and analysed in section 3. Mostly the numerical results will be shown, however some basic experimental data from the wind tunnel will also be presented. Section 4 will be devoted to physical interpretation of simulation results, a discussion, and conclusions.

2. Numerical and laboratory simulation techniques

2.1. Large eddy simulation

According to the LES methodology described, for example, in Lesieur and Métais [32], and Piomelli and Chasnov [33], motions in the simulated turbulent flow are subdivided into the larger-scale, resolved motions that are directly calculated in the nodes of the simulation domain and the smaller-scale, so-called subgrid motions, the integral effect of which is modelled through additional terms in the governing equations for the quantities representing the resolved motions:

$$\frac{\partial \bar{u}_i}{\partial t} + \frac{\partial \bar{u}_j \bar{u}_i}{\partial x_j} = -\frac{\partial \pi}{\partial x_i} + \beta(\bar{T} - T_0)\delta_{i3} + \frac{\partial}{\partial x_j}\left[\nu\left(\frac{\partial \bar{u}_i}{\partial x_j} + \frac{\partial \bar{u}_j}{\partial x_i}\right) - \tau_{ij}\right] \tag{1}$$

$$\frac{\partial \bar{u}_i}{\partial x_i} = 0 \tag{2}$$

$$\frac{\partial \bar{T}}{\partial t} + \frac{\partial \bar{u}_i \bar{T}}{\partial x_i} = \frac{\partial}{\partial x_i}\left(\mu \frac{\partial \bar{T}}{\partial x_i} - Q_i\right) \tag{3}$$

where t stands for the time, $x_i = (x, y, z)$ are the right-hand Cartesian coordinates, $\bar{u}_i = (\bar{u}, \bar{v}, \bar{w})$ are the resolved-scale components of the velocity vector, $\bar{T}$ is the resolved-scale temperature, T_0 is the reference temperature, ν is the kinematic viscosity, and μ is the molecular thermal diffusivity. The quantities $\tau_{ij} = \overline{u_i u_j} - \bar{u}_i \bar{u}_j$ and $Q_i = \overline{T u_i} - \bar{T}\bar{u}_i$ are the subgrid stress and subgrid heat flux, respectively, and $\beta = g/T_0$ is the buoyancy parameter, where g is the gravity acceleration. The overbar signifies the average over the grid-cell volume which in our case is taken to be the filter procedure for separation of the resolved-scale component of motion from

JoT 2 (2001) 007

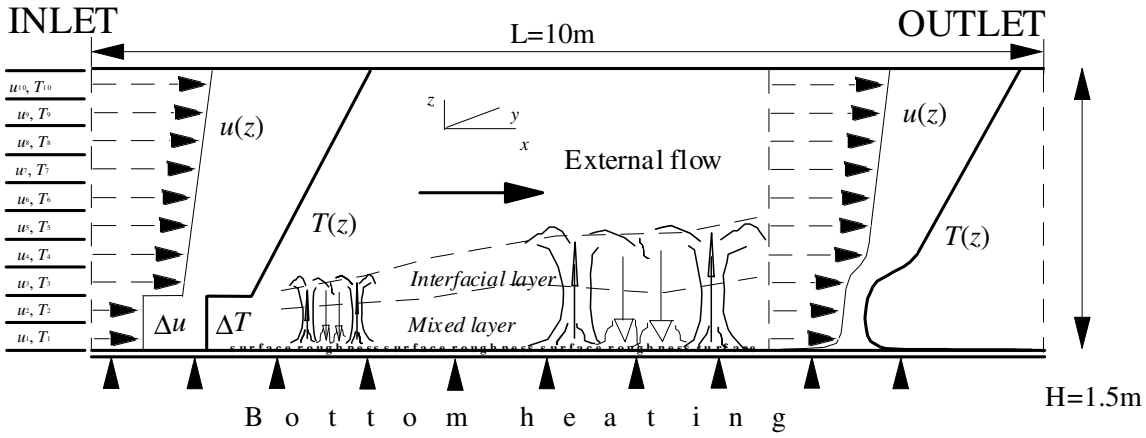

Figure 1. Experimental set-up for simulation of the horizontally evolving CBL. The numerical simulation domain represents the test section of the UniKa wind tunnel.

the subgrid-scale component. The normalized pressure π in equation (1) is defined as

$$\pi = \frac{\bar{p} - p_0}{\rho_0}$$

where $\bar{p}$ is the resolved pressure; p_0 and ρ_0 are the reference values of pressure and density, respectively. The Boussinesq approximation is used in equation (1) to account for the buoyancy forcing. The Coriolis force, which is not important in the considered CBL case (Fedorovich *et al* [21]), is neglected in equation (1).

In the employed LES code, the subgrid stress and heat flux are parametrized in terms of an eddy viscosity and eddy diffusivity model of Deardorff [34], where the eddy viscosity K_m and diffusivity K_h are expressed through the mixing length l and subgrid kinetic energy E:

$$K_m = 0.12 l E^{1/2} \qquad K_h = (1 + 2l/\Delta) K_m \tag{4}$$

where $\Delta = (\Delta x \Delta y \Delta z)^{1/3}$ is the effective grid cell size and l is evaluated depending on the local temperature gradient as

$$l = \begin{cases} \Delta & \text{if } \partial\bar{T}/\partial z \le 0 \\ \min\{\Delta, 0.5E^{1/2}/[\beta(\partial\bar{T}/\partial z)]^{1/2}\} & \text{if } \partial\bar{T}/\partial z > 0. \end{cases} \tag{5}$$

The subgrid kinetic energy E is obtained from a supplementary balance equation. For further details regarding the subgrid model the reader is referred to Nieuwstadt and Brost [15] and Fedorovich *et al* [26], where the adequacy of the employed subgrid model for the considered type of convective flow is demonstrated.

In order to simplify the mathematical notation further, the overbars will be omitted hereafter in the notation for the resolved-scale variables.

A few words should be said about the numerical procedure and boundary conditions. The LES equations (1)–(3) are discretized in the rectangular computational domain on a staggered grid with uniform spacing. In this domain, a right-hand coordinate system is defined with the longitudinal axis X directed from the inlet to the outlet, the horizontal axis Y oriented perpendicular to the flow, and the vertical axis Z directed upwards from the floor to the ceiling, see figure 1. In the current version of the code, the grid consists of $400 \times 60 \times 60$ cubic cells.

JoT 2 (2001) 007

This provides $\Delta = 2.5$ cm for the effective grid cell size in the physical domain corresponding to the test section of the UniKa wind tunnel.

According to the estimates by Kaiser and Fedorovich [22], characteristic values of the integral length scale, the Taylor microscale, and the Kolmogorov microscale in the wind tunnel CBL are, respectively, 50 cm, 1 cm, and 0.1 cm. The Taylor micro time scale is about 0.1 s, the convective turnover time scale is about 2 s, and the flow deformation time scale is of the order of 50 s. The spatial discretization on the grid is of the second order in space. The time advancement is carried out by means of the leapfrog explicit time integration scheme with a weak time filter.

Adjustment of the velocity fields to enforce the conservation of mass in the simulated flow is realized by the pressure. A Poisson equation for π is constructed by combining the continuity and momentum balance equations as is done in Nieuwstadt [35]. This Poisson equation is solved numerically by the fast Fourier transform technique over the horizontal planes, and by tridiagonal matrix decomposition in the vertical direction. In the Fourier series expansions, only cosine functions are used to enable matching the Neumann boundary conditions at the sidewalls.

With respect to the boundary conditions, we try to simulate as realistically as possible the actual conditions in the test section of the UniKa wind tunnel. At the sidewalls and at the ceiling of the test section, no-slip boundary conditions for the velocity and zero-gradient conditions for the temperature, subgrid energy, and pressure are prescribed. The log-wall law is employed to calculate local near-wall turbulent shear stresses, through which the mechanical production of E at the wall is expressed. At the heated bottom surface, the Monin–Obukhov similarity relations are used point by point to couple local thermal and dynamic parameters of the flow. The roughness lengths of walls, floor, and ceiling of the domain are set as external parameters.

The values of u, v, w, and T at the test section inlet (the inflow boundary) are prescribed. These inlet values are decomposed in two parts. The first part (the stationary part) is a steady value corresponding to the settings of the tunnel control system for each particular flow configuration. The second part represents a non-stationary fluctuating component of the inflow. These fluctuations are specified as normally distributed non-correlated random values with a given variance, which is estimated from the measured temperature and velocity fluctuations at the first measurement location in the tunnel. The employed method of prescribing the inlet boundary conditions is considered in detail in Fedorovich *et al* [26].

The radiation boundary condition, also called the convective (or advective) boundary condition, is used at the domain outlet. For the pressure field, the Neumann boundary conditions are set at both the inlet and outlet.

2.2. Wind tunnel experimental set-up

The UniKa thermally stratified wind tunnel has been specially designed as a facility for simulating the inversion-capped CBL developing over a heated underlying surface. A comprehensive description of the tunnel is given in Rau *et al* [36], and Rau and Plate [37].

The tunnel is of close-circuit type, with a 10 m $\times$ 1.5 m $\times$ 1.5 m test section. The return section of the tunnel is subdivided into ten individually insulated layers. Each layer is driven by its own fan and heating system. This allows pre-shaping of the velocity and temperature profiles at the test section inlet as shown in figure 1. A feedback control system enforces quasi-stationary inlet conditions for the flow entering the test section. The test section floor, which is constructed of aluminium plates, can also be heated with a controlled energy input to produce a constant heat flux through the underlying surface.

The components of flow velocity in the tunnel are measured by means of laser Doppler velocimetry (LDV). For temperature measurements, a resistance-wire technique is employed. In addition to these measurements, a laser light sheet technique is applied to visualize two-dimensional flow patterns on planes oriented along various directions with respect to the flow.

JoT 2 (2001) 007

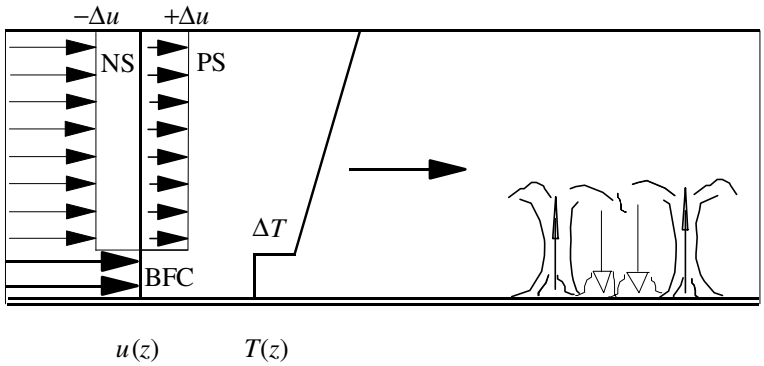

Figure 2. Investigated CBL flow regimes with elevated shears of different signs. The inflow velocity profile in the BFC with zero elevated shear is shown by the bold line. The velocity profile with positive elevated shear is indicated as PS and the profile with negative shear as NS. Note that the initial magnitude of the velocity increment across the inversion in the PS and NS cases is the same.

For more information about the flow measurement and visualization technique employed in the tunnel see Fedorovich *et al* [21], Kaiser and Fedorovich [22], and Fedorovich and Kaiser [23].

3. Flow dynamics in the horizontally evolving CBL

3.1. Investigated flow cases

The reference CBL flow configuration, to which we shall relate numerical and laboratory simulation results discussed in the present paper, will be referred to as the basic flow configuration (BFC, see figure 2).

In the corresponding experimental set-up of the wind tunnel, the two lower layers of the tunnel, with a depth of 0.3 m in total, operate in the open-circuit regime. The incoming flow in these two layers possesses the temperature of the ambient air (about 300 K). The kinematic heat flux through the bottom of the test section is kept constant, at the level of approximately 1 K m s^{-1}. Between the second and the third layers a 30 K temperature jump is imposed. The temperature of each of the subsequent layers is controlled in such a way so as to produce a temperature gradient of 33 K m^{-1} (5 K/layer) in the upper flow region. The flow velocity in all layers at the inlet is set equal to 1 m s^{-1}. The same set of inflow parameters has been prescribed in the numerical simulations for the stationary flow component at the inlet of the LES domain (see section 2.1).

Parameters of the CBL turbulence regime in the BFC case are thoroughly discussed in Fedorovich *et al* [21], Kaiser and Fedorovich [22], Fedorovich and Kaiser [23], and Fedorovich *et al* [26].

Additionally to the BFC case, two CBL flow cases with elevated wind shears have been investigated in the present study. The first case denoted as PS in figure 2 corresponds to the CBL with positive elevated shear. In this case, the longitudinal velocity u at the inlet increases from 1.0 m s^{-1} below the level of capping temperature inversion ($z = 0.3$ m) to a value of 1.5 m s^{-1} in the stably stratified fluid above the inversion. In the second case of negative elevated shear (NS in figure 2), the incoming flow velocity is kept equal to 1.0 m s^{-1} below the inversion level and reduces to 0.5 m s^{-1} above it. Thus, the magnitude of imposed velocity shear in the PS and NS cases is the same, 0.5 m s^{-1}.

JoT 2 (2001) 007

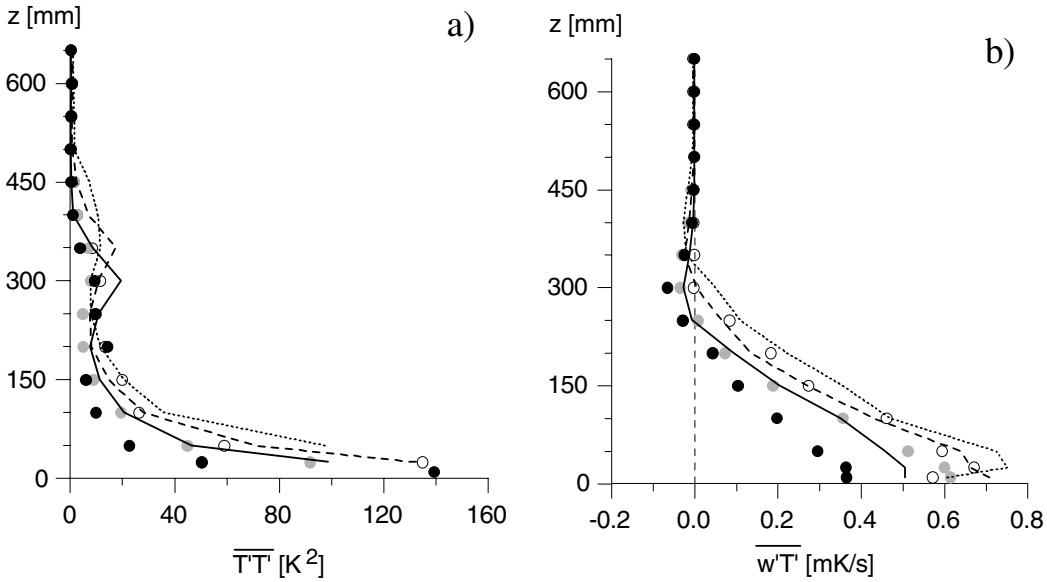

Figure 3. Temperature variance (a) and vertical kinematic heat flux (b) measured in the wind tunnel CBL with positive shear across the inversion (PS case, points) and with shear-free inversion (BFC case, curves). Data refer to the following distances from the tunnel inlet: $x = 3.98$ m (full curves and black symbols), $x = 5.63$ m (dashed curves and grey symbols), and $x = 7.28$ m (dotted curves and open symbols).

The remaining flow parameters in both cases are kept equal to their BFC values. Unfortunately, the NS case cannot be reproduced in the UniKa wind tunnel within its present operating ranges. Therefore, the comparison of numerical results with the wind tunnel data is possible only for the BFC and PS cases.

3.2. Attenuation of the CBL growth by positive elevated shear: experimental evidence

The extreme negative value of the entrainment heat flux at the CBL top is usually considered as an indicator of the CBL upper interface and the corresponding elevation is taken as the CBL depth mark and as the CBL turbulence length scale (Deardorff [38], Fedorovich and Mironov [39]). The temperature variance maximum that is approximately co-located with the heat flux minimum within the entrainment layer is also often used for identification of the CBL top (Fedorovich *et al* [21]).

Evolution of temperature variance $\overline{T'^2}$ and vertical kinematic heat flux $\overline{w'T'}$ profiles along the tunnel in the BFC and PS cases is demonstrated in figure 3. Note that turbulence statistics in the horizontally inhomogeneous wind tunnel CBL are calculated by time averaging. Therefore, the overbars in the above expressions signify the time averages, not the filtering operation that has been used for velocity and temperature fields in equations (1)–(3) and the primes, consequently, denote deviations from these time averages.

Changes of both statistics along the wind tunnel reveal the progressive growth of the CBL depth as a function of x in the case without elevated shear (BFC). On the other hand, the CBL depth does not significantly vary along the tunnel in the PS case. This may be inferred from practically constant elevations of both heat flux minima and temperature variance maxima within the entrainment zone of the simulated CBL.

JoT 2 (2001) 007

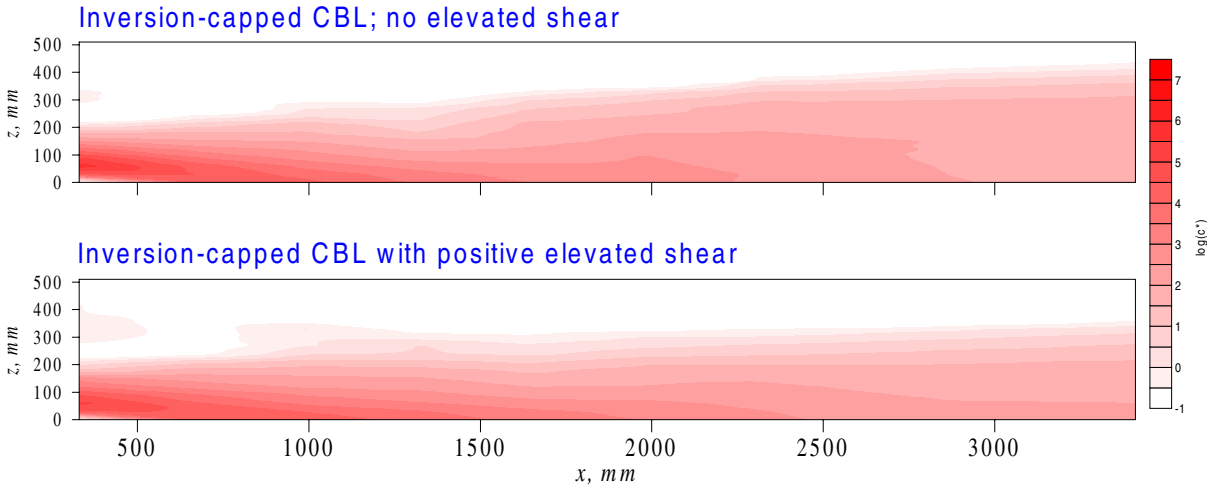

Figure 4. Concentration distributions of gaseous tracer from a point source in the CBL case with shear-free capping inversion (BFC case, upper plot) and in the case of positive shear across the capping inversion (PS case, lower plot). The source elevation is 100 mm. The longitudinal distance is counted from the source location. Concentration values are given in dimensionless units obtained with the same set of scales for both cases.

Additional evidence regarding the attenuation of the CBL growth rate by positive elevated shear has been acquired from wind tunnel experiments on the gaseous tracer dispersion in the horizontally evolving CBL. In figure 4, a two-dimensional cross section of the concentration field of the tracer emitted from a point source in the CBL with positive elevated shear (PS case) is compared with the concentration distribution in the BFC (no elevated shear). The source strength and location are identical in the both cases. The comparison of concentration patterns clearly shows that the depth of the convectively mixed flow region filled with tracer grows noticeably faster along the tunnel in the PS case than in the BFC case.

3.3. Numerical simulation of the CBL with elevated shears of opposite sign

Since the blocking effect of positive shear on the CBL growth was first found in the wind tunnel experiments of Fedorovich and Kaiser [22], the authors of the present study attempted to elaborate a physical explanation for it. The first idea was to relate the observed phenomenon to the so-called shear sheltering of turbulence. A theory of turbulence sheltering at an interface separating turbulent and turbulence-free flow regions was proposed by Hunt and Durbin [31]. Based on this theory, Fedorovich *et al* [27] estimated the magnitude of shear sheltering in the PS case and found it to be in reasonable agreement with the wind tunnel observations for this case.

Furthermore, Fedorovich *et al* [26, 27] have complemented experiments in the UniKa wind tunnel with the LES of the horizontally evolving CBL. Results of these numerical simulations for the BFC and PS cases have shown fair agreement with the corresponding wind tunnel data regarding the mean flow parameters and turbulence statistics.

For the NS case, however, the LES data of Fedorovich *et al* [27] have yielded a rather unexpected result. It has turned out that negative shear across the inversion affects the CBL evolution in the opposite way as compared to the positive elevated shear: the CBL growth in the NS case occurs faster than that in the BFC case. This result is in contradiction with

JoT 2 (2001) 007

the theory of Hunt and Durbin [31] that predicts the shear sheltering to be independent of the direction of shear across the interface separating the turbulent and non-turbulent fluids.

In order to gain a deeper insight into the mean flow and turbulence structure of the horizontally evolving CBL with elevated wind shears of opposite sign, a series of new LES experiments has been conducted. Results of these experiments are presented and discussed below. In the simulations performed, all basic parameters of the NS, BFC, and PS cases have been kept as they are given in section 3.1, but the initial inversion elevation has been slightly increased, up to 0.375 m. This allowed us to accommodate additional computational grid points in the mixed core of the CBL.

Temperature distributions along the central XoZ plane of the simulation domain for all three investigated cases are compared in figure 5. In the upper group of plots, the instantaneous temperature fields are presented. In the lower group of plots, the time-averaged temperature distributions are shown. The averaging approach employed for the calculation of turbulence statistics in the simulated flow is described in Fedorovich *et al* [26].

Let us first consider the development of the temperature field in the BFC case with no elevated shear. At the early stages of the CBL evolution (small x values), the vertical distribution of temperature is characterized by the presence of the sharp capping inversion that separates the less buoyant premixed fluid in the lower portion of the flow and the linearly stratified fluid aloft. A thin rugged sublayer with warm air develops close to the heated underlying surface. In the mean temperature pattern, this sublayer appears like a pillow of hot air. The buoyantly generated turbulence has not yet developed to mix up the air below the capping inversion.

The depth of the zone warmed by convective heat transfer from the surface gradually increases downwind whilst the dimensions of the rising convective plumes grow. The growing plumes get detached from each other and the zones of cooler descending air appear between them.

Within the fetch range 2.5 m $< x <$ 4 m, the CBL passes through the transition stage that has been the subject of special investigation in Fedorovich *et al* [26]. During the transition, the release of potential energy accumulated in the unstable flow at the stage of pre-mixed CBL triggers the active mixing in the flow region below the inversion. The activated vertical turbulent motions strongly perturb the inversion and stimulate the entrainment of the warm air from the quiescent flow above the inversion down into the convectively mixed layer.

Downwind of the transition zone ($x > 4$ m), the instantaneous temperature pattern consists of vast areas with relatively low temperatures (they correspond to slow and broad downdrafts) separated by comparatively narrow columns of warmer air (they, in turn, correspond to fast rising convective thermals). Such correlation between the instantaneous temperature and vertical velocity patterns in the simulated CBL is demonstrated and discussed in Fedorovich *et al* [26]. The capping inversion in the post-transition phase progressively weakens due to erosion caused by the rising thermals. The mean temperature distribution for the BFC case allows us to conclude that in the absence of the elevated shear the overall CBL depth slowly increases with distance.

The comparison of temperature patterns for the NS and PS cases with the temperature distributions for the BFC case reveals the effect of elevated velocity shears on the CBL thermal structure, see figure 5. The average height achieved by the penetrative convective thermals in the case of negatively sheared inversion is obviously larger than in the BFC case with no elevated shear. In the PS case, the situation is the opposite: the thermals penetrate considerably lower into the external stably stratified fluid than in the BFC case.

The mean temperature distributions in figure 5 provide additional support for the above conclusions regarding the CBL growth dynamics. The core region of the CBL with almost

JoT 2 (2001) 007

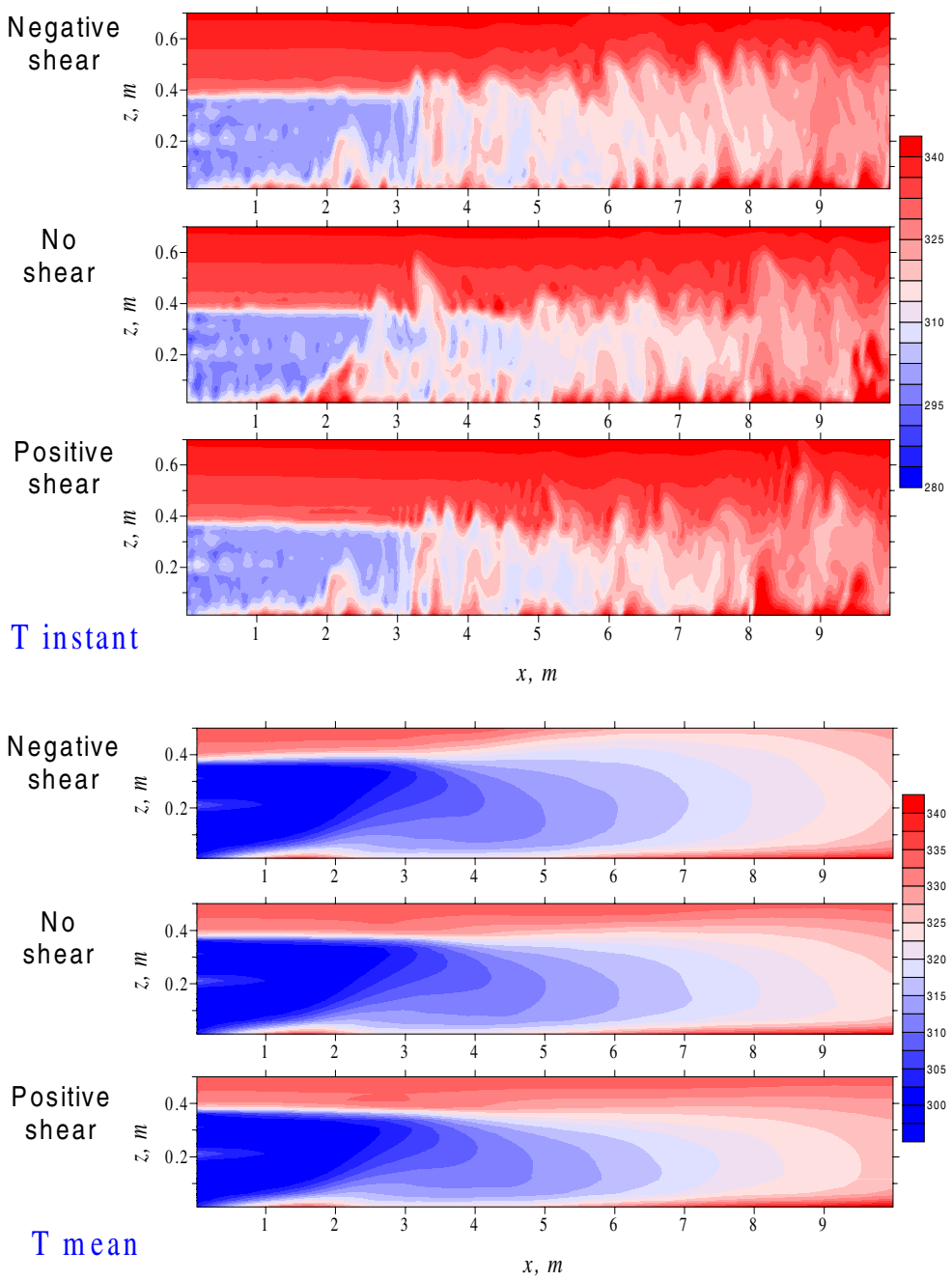

Figure 5. Instantaneous (upper three plots) and mean (lower three plots) temperature distributions along the simulated CBL with negative elevated shear (NS case), no elevated shear (BFC case), and positive elevated shear (PS case).

uniform vertical temperature distribution deepens with distance noticeably faster in the NS case than in the BFC case. On the other hand, the CBL growth is substantially slowed down, not to say practically stopped, in the presence of positive elevated shear.

In all three flow cases studied, the heat transport associated with convective entrainment at the CBL top is directed downwards, from the flow region with warmer air above the inversion

JoT 2 (2001) 007

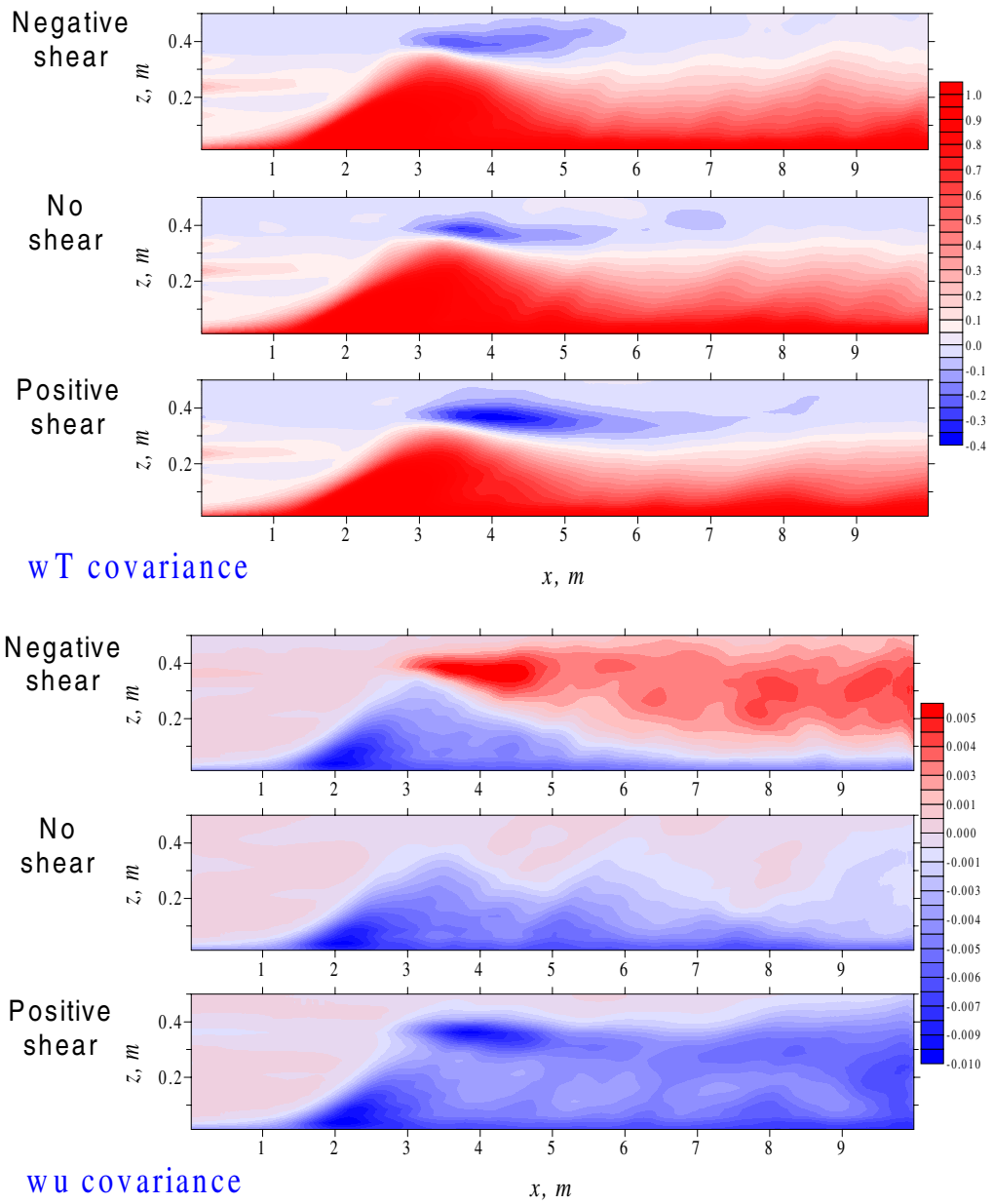

Figure 6. Distributions of the vertical kinematic turbulent fluxes of heat (upper three plots) and momentum (lower three plots) along the simulated CBL with negative elevated shear (NS case), no elevated shear (BFC case), and positive elevated shear (PS case).

down into the CBL. From this point of view, all these cases are qualitatively equivalent.

In order to clarify this issue, we present simulated distributions of the vertical kinematic heat flux along the CBL (the upper three plots in figure 6). Despite certain quantitative dissimilarities between the $\overline{w'T'}$ fields for the NS, BFC, and PS cases, they demonstrate common general features: the activation of entrainment of heat at the lee side of the transition region and gradual vanishing of the negative entrainment flux down the flow as the capping inversion erodes. At the same time, the horizontal variations of height, at which the entrainment flux magnitude reaches

JoT 2 (2001) 007

its maximum (it can be taken as the indicator of the CBL upper interface, see section 3.1), certify that the CBL growth rates in the three cases considered are not the same. The flow region with negative $\overline{w'T'}$ values downwind of the transition zone (it appears as a blue plume in the presented plots) is tilted slightly upwards in the NS case and slightly downwards in the PS case, whereas in the BFC case it is almost parallel to the surface.

However, when it comes to the properties of momentum transport in the upper portion of the CBL, the three simulated situations demonstrate principally different features.

In the case of negative elevated shear, the covariance $\overline{w'u'}$ (that is the vertical component of the turbulent kinematic momentum flux) is positive at the capping inversion level, and therefore the turbulent transport of momentum across the inversion is directed upwards (see the uppermost figure from the lower group of plots in figure 6). This transport mechanism may also be interpreted as entrainment of negative mean momentum across the inversion down into the convectively mixed layer. In the case of positive elevated shear (the lowermost plot in figure 6), the momentum is transported downwards across the capping inversion (the $\overline{w'u'}$ values are negative). Thus, in this case the positive mean momentum is entrained into the CBL from the faster moving fluid aloft. As might be expected, the momentum flux distribution in the CBL with the shear-free capping inversion (the BFC case, second plot from below in figure 6) does not point to any significant turbulent transport of momentum across the inversion.

Note that in all three cases under consideration the values of negative momentum flux associated with turbulent friction at the underlying surface do not differ very much, see the three lower plots in figure 6.

The momentum transport across the inversion adversely affects the mean flow inside the CBL in the cases of positive and negative elevated shear. The entrainment of negative momentum in the NS case leads to the progressive decrease of mean velocity in the convectively mixed flow region below the inversion. This decrease can be observed in the mean u distribution for the NS case (the uppermost plot in figure 7). In the presence of positive elevated shear (the PS case), the mean flow inside the CBL noticeably accelerates along x due to the entrainment of positive momentum into the CBL from the outer flow with higher velocity. The increase of mean velocity with distance below the inversion is clearly seen in the u pattern for the PS case (the third plot from the top in figure 7). Without elevated shear, the mean horizontal velocity field has almost zero longitudinal variability throughout the CBL, see the second plot from the top in figure 7.

Based on the mass conservation considerations, one has to assume that the identified longitudinal changes of the mean horizontal velocity in the PS and NS are accompanied with generation of mean motions in other directions. Due to flow symmetry with respect to the central XoZ plane of the simulation domain, the mean transversal velocity in this plane should be close to zero. Computed distributions of the y component of the mean flow velocity along the domain (not shown) indicate that this component of mean motion is indeed negligibly weak. At the same time, the induced mean vertical motion associated with acceleration/deceleration of the CBL flow below the inversion can be easily identified in the central XoZ plane, see patterns of mean w in figure 7.

While considering distributions of mean w along the tunnel, it should be kept in mind that the characteristic magnitude of w fluctuations corresponding to the convective turbulent motions in the main portion of the CBL (about 0.2 m s^{-1}) is considerably larger than typical values of mean w in figure 7. Nevertheless, as we will see from the following analysis of the LES data, the role of organized vertical motion becomes important within the capping inversion layer, where it is superimposed with the convective entrainment.

The presented mean vertical velocity distributions for the NS, BFC, and PS cases (in the order from the top to the bottom in the lower group of plots in figure 7) have much in common

JoT 2 (2001) 007

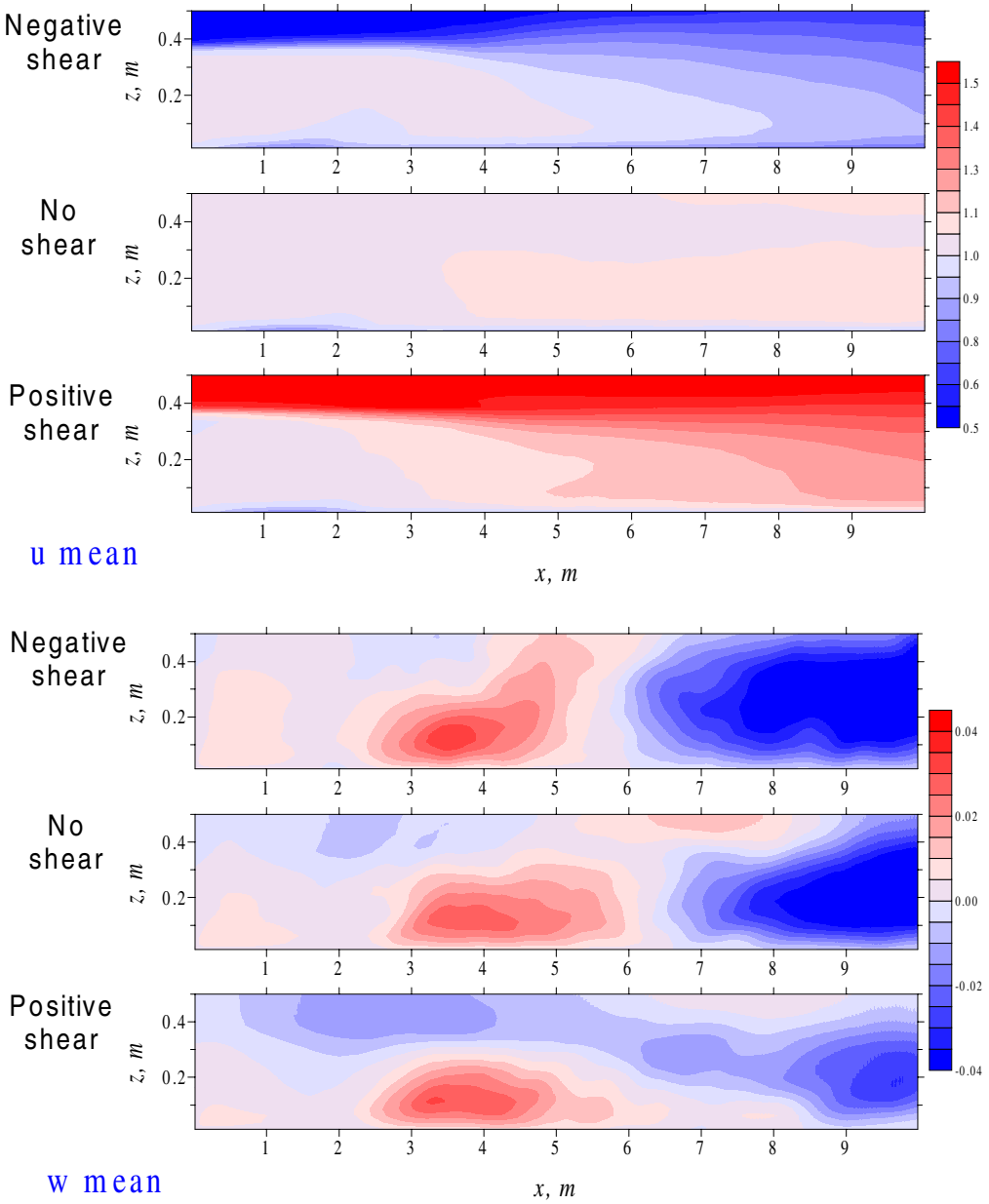

Figure 7. Distributions of the horizontal (upper three plots) and vertical (lower three plots) mean velocity components along the simulated CBL with negative elevated shear (NS case), no elevated shear (BFC case), and positive elevated shear (PS case).

in the flow below the inversion and during the transition, when the release of potential energy accumulated at the pre-transition stage (see the discussion in Fedorovich *et al* [27]) causes active upward motions with non-zero mean component.

Downwind of the transition zone (at $x > 4$ m), the features of mean vertical velocity distributions in the three investigated cases are rather different. In the case of negative elevated shear, the area with positive mean vertical motion extends through the inversion layer deep into the outer flow region. The ascending mean motion pushes the capping inversion upwards in

JoT 2 (2001) 007

addition to the convective entrainment that drives the inversion in the same direction. In the absence of elevated shear (the BFC case), the magnitude of mean vertical motion at the level of inversion is vanishingly small. Under such conditions, the CBL grows almost exclusively by convective entrainment. As we have seen in the plots of temperature and kinematic heat flux (figures 5 and 6), this growth is noticeably smaller than in the case of negative elevated shear.

In the case of positive elevated shear, the flow acceleration below the inversion leads to the downward mean vertical motion at the inversion level. The blue belt of negative mean w values along the inversion in the PS case is clearly seen in the lowermost plot of figure 7. This belt is an indicator of local subsidence at the CBL top that opposes the entrainment and slows down the CBL growth compared to the CBL case with shear-free inversion.

4. Discussion and conclusions

The reported study has focused on the role of elevated wind shears on the growth dynamics of horizontally evolving CBL and properties of vertical transport across the sheared density interface (the capping inversion) at the CBL top.

Three CBL flow configurations have been investigated. In the first configuration, which is the case of negative wind shear across the inversion (we have also called it negative elevated shear, NS), the flow above the capping inversion possessed a smaller momentum than mean motion in the convectively mixed region of the CBL. The second configuration corresponded to the reference (basic) CBL flow case (BFC) with no mean velocity increment across the capping inversion. In the third configuration, the flow above the capping inversion possessed a larger momentum than mean motion in the convectively mixed flow. This was the case of positive shear across the capping inversion or positive elevated shear (PS). The magnitudes of the initial across-inversion velocity increments in the NS and PS cases were equal.

The effect of negative elevated shear on the CBL growth was found to be opposite to the effect of positive elevated shear. In the NS case, the CBL growth was enhanced compared to that observed in the BFC case, while the CBL growth rate in the PS case was noticeably smaller that in the BFC case.

In their recent paper regarding evolution of CBL with elevated wind shears, Fedorovich *et al* [27] explained the aforementioned effects by different impacts of negative versus positive wind shears on convective thermals penetrating into the stably stratified flow with higher (in the PS case) and lower (in the NS case) mean momentum than the momentum of the CBL flow. The explanation was based on the analysis of particular characteristics of the CBL turbulence structure as modified by elevated wind shears of opposite sign.

Results of the present study suggest that Fedorovich *et al* [27] have correctly identified the modifications of turbulence structure in the CBL with sheared capping inversion but overlooked the main effect of elevated wind shear on the flow dynamics in horizontally evolving CBL. This main effect is associated with local organized vertical motions at the CBL top due to acceleration or deceleration of the CBL flow caused by the turbulent transport of momentum across the sheared capping inversion.

The acceleration of the CBL flow (the increase of the u component of mean motion with x below the capping inversion) takes place in the PS case. Due to the fluid continuity it produces negative (descending) mean vertical motion at the level of inversion. The opposite happens in the NS case, when the upward transport of momentum across the inversion leads to deceleration of mean flow within the CBL. This deceleration leads to positive (ascending) organized vertical motion pushing the capping inversion upwards.

The generated vertical motion component differently interacts with convective turbulent entrainment at the CBL top in the NS and PS cases. In the NS case, the organized upward motion

JoT 2 (2001) 007

contributes to the CBL growth in addition to the entrainment growth mechanism. In contrast, the organized downward motion in the PS case opposes the entrainment and thus slows down the CBL growth.

The discussed effect of elevated wind shear on the CBL flow dynamics leaves open the problem of experimental verification of the Hunt and Durbin [31] theory of turbulence shear sheltering in the case of a CBL-type flow. In the studied cases of the horizontally inhomogeneous CBL, the impact of generated mean vertical motion on the growth of the turbulent flow region (that is the convectively mixed layer in our case) has apparently been much stronger than any second-order effect associated with modification of turbulent exchange across the inversion layer by mean flow shear. In order to single out and evaluate the direct influence of elevated wind shear on the penetration of convective turbulent motions through the capping inversion, one has to investigate the fine structure of turbulence within the sheared capping inversion at the top of a non-steady and horizontally quasi-homogeneous CBL.

Acknowledgments

Financial support provided by the Deutsche Forschungsgemeinschaft (DFG) within the Project 'Untersuchung und Parametrisierung der Wechselwirkungen von Skalen der Turbulenz konvektiver Grenzschichtströmungen unter Verwendung einer einheitlichen Datengrundlage aus Naturmessungen, Windkanalversuchen und numerischen Modellen' is gratefully acknowledged. The authors are thankful to Paul Linden, Jakob Mann, Dmitrii Mironov, and Frans Nieuwstadt for their attention to the study and stimulating discussions.

References

[1] Clarke R H, Dyer A J, Brook R R, Reid D G and Troup A J 1971 The Wangara experiment: boundary layer data *Technical Paper* 19, Div. Meteor. Phys. CSIRO Australia, p 363
[2] Kaimal J C, Wyngaard J C, Haugen D A, Coté O R, Izumi Y, Caughey S J and Readings C J 1976 Turbulence structure in a convective boundary layer *J. Atmos. Sci.* **33** 2152–69
[3] Caughey S J and Palmer S G 1979 Some aspects of turbulence structure through the depth of the convective boundary layer *Q. J. R. Meteor. Soc.* **105** 811–27
[4] Lenschow D H, Wyngaard J C and Pennel W T 1980 Mean-field and second-momentum budgets in a baroclinic, convective boundary layer *J. Atmos. Sci.* **37** 1313–26
[5] Deardorff J W, Willis G E and Lilly D K 1969 Laboratory investigation of non-steady penetrative convection *J. Fluid Mech.* **35** 7–31
[6] Deardorff J W, Willis G E and Stockton B H 1980 Laboratory studies of the entrainment zone of a convectively mixed layer *J. Fluid Mech.* **100** 41–64
[7] Willis G E and Deardorff J W 1974 A laboratory model of the unstable planetary boundary layer *J. Atmos. Sci.* **31** 1297–307
[8] Deardorff J W and Willis G E 1985 Further results from a laboratory model of the convective planetary boundary layer *Bound.-Layer Meteor.* **32** 205–36
[9] Adrian R J, Ferreira R T D S and Boberg T 1986 Turbulent thermal convection in wide horizontal fluid layers *Experiments in Fluids* vol 4 (Berlin: Springer) pp 121–41
[10] Kumar R and Adrian R J 1986 Higher order moments in the entrainment zone of turbulent penetrative thermal convection *J. Heat Transfer* **108** 323–9
[11] Cenedese A and Querzoli G 1994 A laboratory model of turbulent convection in the atmospheric boundary layer *Atmos. Environ.* **28** 1901–14
[12] Deardorff J W 1972 Numerical investigation of neutral and unstable planetary boundary layers *J. Atmos. Sci.* **29** 91–115
[13] Moeng C-H 1984 A large-eddy simulation for the study of planetary boundary layer turbulence *J. Atmos. Sci.* **41** 2052–62
[14] Wyngaard J C and Brost R A 1984 Top–down and bottom–up diffusion of a scalar in the convective boundary layer *J. Atmos. Sci.* **41** 102–12
[15] Nieuwstadt F T M and Brost R A 1986 Decay of convective turbulence *J. Atmos. Sci.* **43** 532–46

JoT 2 (2001) 007

[16] Mason P J 1989 Large-eddy simulation of the convective atmospheric boundary layer *J. Atmos. Sci.* **46** 1492–516
[17] Schmidt H and Schumann U 1989 Coherent structure of the convective boundary layer derived from large-eddy simulations *J. Fluid Mech.* **200** 511–62
[18] Mason P J 1992 Large-eddy simulation of dispersion in convective boundary layers with wind shear *Atmos. Environ.* A **26** 1561–71
[19] Moeng C-H and Sullivan P P 1994 A comparison of shear-and buoyancy-driven planetary boundary layer flows *J. Atmos. Sci.* **51** 999–1022
[20] Khanna S and Brasseur J G 1998 Three-dimensional buoyancy- and shear-induced local structure of the atmospheric boundary layer *J. Atmos. Sci.* **55** 710–43
[21] Fedorovich E, Kaiser R, Rau M and Plate E 1996 Wind tunnel study of turbulent flow structure in the convective boundary layer capped by a temperature inversion *J. Atmos. Sci.* **53** 1273–89
[22] Kaiser R and Fedorovich E 1998 Turbulence spectra and dissipation rates in a wind tunnel model of the atmospheric convective boundary layer *J. Atmos. Sci.* **55** 580–94
[23] Fedorovich E and Kaiser R 1998 Wind tunnel model study of turbulence regime in the atmospheric convective boundary layer *Buoyant Convection in Geophysical Flows* ed E J Plate *et al* (Dordrecht: Kluwer) pp 327–70
[24] Ohya Y, Hayashi K, Mitsue S and Managi K 1998 Wind tunnel study of convective boundary layer capped by a strong inversion *J. Wind Eng.* **75** 25–30
[25] Ohya Y and Uchida T 1999 Wind tunnel study and DNS of stable boundary layers and convective boundary layers in the atmosphere *Turbulence and Shear Flow Phenomena* vol 1, ed S Banerjee and J K Eaton (Begell House) pp 589–94
[26] Fedorovich E, Nieuwstadt F T M and Kaiser R 2001 Numerical and laboratory study of horizontally evolving convective boundary layer. Part I: Transition regimes and development of the mixed layer *J. Atmos. Sci.* **58** 70–86
[27] Fedorovich E, Nieuwstadt F T M and Kaiser R 2001 Numerical and laboratory study of horizontally evolving convective boundary layer. Part II: Effects of elevated wind shear and surface roughness *J. Atmos. Sci.* **58** 546–60
[28] Csanady G T 1978 Turbulent interface layers *J. Geophys. Res.* **83** 2329–42
[29] Jacobs R G and Durbin P A 1998 Shear sheltering and the continuous spectrum of the Orr–Sommerfeld equation *Phys. Fluids* **10** 2006–11
[30] Hunt J C R 1998 Eddy dynamics and kinematics of convective turbulence *Buoyant Convection in Geophysical Flows* ed E J Plate *et al* (Dordrecht: Kluwer) pp 41–82
[31] Hunt J C R and Durbin P A 1999 Perturbed vortical layers and shear sheltering *Fluid Dynam. Res.* **24** 375–404
[32] Lesieur M and Métais O 1996 New trends in large-eddy simulations of turbulence *Ann. Rev. Fluid Mech.* **28** 45–82
[33] Piomelli U and Chasnov J R 1996 Large-eddy simulations: theory and applications *Turbulence and Transition Modelling* ed M Hallbäck *et al* (Dordrecht: Kluwer) pp 269–336
[34] Deardorff J W 1980 Stratocumulus-capped mixed layers derived from a three-dimensional model *Bound.-Layer Meteor.* **18** 495–527
[35] Nieuwstadt F T M 1990 Direct and large-eddy simulation of free convection *Proc. 9th Int. Heat Transfer Conf.* (American Society of Mechanical Engineering) pp 37–47
[36] Rau M, Bächlin W and Plate E 1991 Detailed design features of a new wind tunnel for studying the effects of thermal stratification *Atmos. Environ.* A **25** 1258–63
[37] Rau M and Plate E J 1995 Wind tunnel modelling of convective boundary layers *Wind Climate in Cities* ed J Cermak *et al* (Dordrecht: Kluwer) pp 431–56
[38] Deardorff J W 1970 Convective velocity and temperature scales for the unstable planetary boundary layer and for Raleigh convection *J. Atmos. Sci.* **27** 1211–13
[39] Fedorovich E E and Mironov D V 1995 A model for shear-free convective boundary layer with parametrized capping inversion structure *J. Atmos. Sci.* **52** 83–95

JoT 2 (2001) 007